Computing solubility and thermodynamic properties of H_2O_2 in water

Saji, Tijin H.G.; Vicent-Luna, José Manuel; Vlugt, Thijs J.H.; Calero, Sofía; Bagheri, Behnaz

DOI
10.1016/j.molliq.2024.124530

Publication date
2024

Document Version
Final published version

Published in
Journal of Molecular Liquids

Journal of Molecular Liquids 401 (2024) 124530

Contents lists available at ScienceDirect

Journal of Molecular Liquids

journal homepage: www.elsevier.com/locate/molliq

Computing solubility and thermodynamic properties of H_2O_2 in water

Tijin H.G. Saji [a,b], José Manuel Vicent-Luna [a], Thijs J.H. Vlugt [c], Sofía Calero [a,*], Behnaz Bagheri [a,b,*]

[a] Department of Applied Physics and Science Education, Technical University of Eindhoven, PO Box 513, 5600 MB, Eindhoven, the Netherlands
[b] Institute for Complex Molecular Systems, PO Box 513, 5600 MB, Eindhoven, the Netherlands
[c] Process & Energy Department, Faculty of Mechanical, Maritime and Materials Engineering, Delft University of Technology, Leeghwaterstraat 39, 2628 CB, Delft, the Netherlands

ARTICLE INFO

Keywords:
Hydrogen peroxide
Aqueous solution
Molecular Dynamics
Continuous Fractional Component Monte Carlo simulations

ABSTRACT

Hydrogen peroxide plays a key role in many environmental and industrial chemical processes. We performed classical Molecular Dynamics and Continuous Fractional Component Monte Carlo simulations to calculate thermodynamic properties of H_2O_2 in aqueous solutions. The quality of the available force fields for H_2O_2 developed by Orabi and English (2018) [67], and by Cordeiro (2014) [69] was systematically evaluated. To assess which water force field is suitable for predicting properties of H_2O_2 in aqueous solutions, four widely used water force fields were used, namely the TIP3P, TIP4P/2005, TIP5P-E, and a modified TIP3P force field. While the computed densities of pure H_2O_2 in the temperature range of 253 - 353 K using the force field by Orabi & English are in excellent agreement with experimental results, the densities using the force field by Cordeiro are underestimated by 3%. The TIP4P/2005 force field in combination with the H_2O_2 force field developed by Orabi & English can predict the densities of H_2O_2 aqueous solution for the whole range of H_2O_2 mole fractions in very good agreement with experimental results. The TIP4P/2005 force field in combination with either of the H_2O_2 force fields can predict the viscosities of H_2O_2 aqueous solutions for the whole range of H_2O_2 mole fractions in reasonably good agreement with experimental results. The computed diffusion coefficients for H_2O_2 and water molecules using the TIP4P/2005 force field with either of the H_2O_2 force fields are almost constant for the whole range of H_2O_2 mole fractions. Hydrogen bond analysis showed a steady increase in the number of hydrogen bonds with the solute concentrations in H_2O_2 aqueous solutions for all combinations except for the Cordeiro-TIP5P-E and Orabi-TIP5P-E systems, which showed a minimum at intermediate concentrations. The Cordeiro force field for H_2O_2 in combination with either of the water force fields can predict the Henry coefficients of H_2O_2 in water in better agreement with experimental values than the force field by Orabi & English.

1. Introduction

Hydrogen peroxide, H_2O_2, has attracted considerable interest as it plays a key role in the oxidative chemistry of the troposphere. It can be found both in the gas and in the aqueous phase [1,2], and has several industrial [3], environmental [4], and biological [5] applications. The recombination of hydroperoxyl (HO_2) radicals is the most important chemical pathway leading to the production of H_2O_2 in the troposphere [6–8]. Subsequently, H_2O_2 can lead to the acidification of clouds, rain, and fog by oxidizing SO_2 and converting it into H_2SO_4 (and to a less extent oxidizing NO_2 and converting it into HNO_3) [9–13]. H_2O_2 also serves as a reservoir of HO_x radicals that are key oxidants in controlling the self-cleaning of the atmosphere [14–16].

H_2O_2 was first synthesized by Thenard [17] by the reaction of barium peroxide with nitric acids in 1818 and is now considered an important reagent of green chemistry since it decomposes to water and oxygen as the only reaction products. This feature makes H_2O_2 an environmentally friendly oxidizing agent for a wide range of applications such as pulp and paper bleaching, textile applications, detergent applications, disinfectant applications, wastewater treatment, and chemical oxidation processes [18,19]. It could also serve as a liquid fuel, an alternative to H_2 and O_2, in a fuel cell [20–22].

* Corresponding authors at: Department of Applied Physics and Science Education, Technical University of Eindhoven, PO Box 513, 5600 MB, Eindhoven, the Netherlands.
E-mail addresses: s.calero@tue.nl (S. Calero), b.bagheri@tue.nl (B. Bagheri).

https://doi.org/10.1016/j.molliq.2024.124530
Received 11 September 2023; Received in revised form 11 March 2024; Accepted 19 March 2024
Available online 28 March 2024

H_2O_2 is currently produced on an industrial scale with the anthraquinone oxidation (AO) process in which hydrogen, atmospheric oxygen, and an anthraquinone derivative (typically 2-alkyl-anthraquinone) are used with the latter acting as a reaction carrier [18,19]. The ubiquitous AO process involves multiple steps which require significant energy input and generates waste. In addition, the transport, storage, and handling of bulk H_2O_2 involve hazards as it is irritating to nose and eyes, and high concentration of H_2O_2 is explosive [23]. Other methods for large-scale production of H_2O_2 include partial oxidation of primary or secondary alcohols, and electrochemical methods [24]. Novel alternatives are under investigation such as direct synthesis of H_2O_2 from O_2 and H_2 using a variety of catalysts like alumina, silica, carbon, solvents (e.g., water) [25,26], photocatalytic reactions over semiconductors where reactive oxygen-based species (e.g., $OH^{\bullet}$, O^{2-}, and H_2O_2) are formed at the surface of semiconductor oxides under UV irradiation [27]. An alternative technology to produce H_2O_2 is to use low temperature (or non-thermal) plasmas [28,29] which allows H_2O_2 production at ambient temperatures and pressures [30–34]. This enables direct delivery of H_2O_2 to different substrates; even to heat sensitive substrates such as living tissues. The latter has led to biomedical applications of low temperature plasmas [35]. For such applications, it is important to know which mechanisms determine the uptake of plasma products (e.g., H_2O_2) in the liquid around the cells and what is the concentration of plasma products in the aqueous phase. For this, information on the solubility and thermodynamic properties of the molecule are necessary so that this can be leveraged into macroscopic plasma fluid models [36] to predict the final concentration of H_2O_2 in the liquid phase. Little information is available on solubility and thermodynamic properties of H_2O_2 in aqueous solutions. The scarcity of this data is especially relevant when temperature and/or pressure changes. The motivation of this work is to provide such data for H_2O_2 using molecular simulations.

Due to the pivotal role of H_2O_2 in many chemical processes, many experimental and computational studies have been conducted to investigate its properties. The crystal structure of H_2O_2 was investigated using diffraction methods or Raman spectroscopy in Refs. [37–41]. Other experimental studies have investigated its densities [42], viscosities [43], vibrational spectra [44,38,45–47], vapor pressures [48] and other thermodynamic properties [49]. In addition, densities, freezing points, and vapor pressures of aqueous H_2O_2 solutions were investigated experimentally in Refs. [42,50–52].

Various computational studies have been carried out which shed light on structural properties of H_2O_2 monomers as well as its clusters, torsional barrier energies, and vibrational-rotational energy levels [53–57] using quantum mechanical approaches. Structure and dynamics of H_2O_2 in water were also investigated using quantum mechanical methods in Refs. [58–60].

In this work, we use force field based Molecular Dynamics (MD) and Continuous Fractional Component Monte Carlo (CFCMC) simulations with the purpose of obtaining solubilities and thermodynamic properties of H_2O_2 in water, for the first time, in a systematic manner such that the quality of the available force fields for H_2O_2 are assessed. Given the complete miscibility of H_2O_2 in water at all concentrations, it is both practical and insightful to explore the properties of H_2O_2 aqueous solutions at varying mole fractions. This allows for a comprehensive understanding of the behavior of the solution at different concentrations.

Although several force fields are available for H_2O_2 [61–64], only a few of them have been parameterized with respect to the interactions between both H_2O_2 - H_2O_2 and H_2O_2 - H_2O. One is the ABEEM/MM, the atom-bond electronegativity equalization fluctuating charge molecular force field [65,66], which is computationally very expensive due to its complex potential energy functional form [65,66]. A simple additive potential model for H_2O_2 was proposed by Orabi & English [67] which was parameterized to account for interactions of H_2O_2 with itself and with water. The model was calibrated with regard to the experimental density and heat of vaporization of pure liquid H_2O_2 at 0 °C, and it was able to reproduce the experimental diffusion coefficient at 0 °C and the heat capacity at 25 °C of liquid H_2O_2. With a combination of the modified TIP3P water force field [68], the H_2O_2 force field could predict the experimental hydration free energies and densities of aqueous H_2O_2 solutions [67]. Another force field parametrization is from the work of Cordeiro [69], wherein the bonded interactions were obtained from *ab initio* quantum calculations [70,54], and the Lennard-Jones parameters and partial charges were modified to reproduce the properties of pure liquid H_2O_2 and its hydration free energy. This force field was used to study the distribution, mobility and residence times of H_2O_2 at the interface of water and phospholipid biomembranes. In addition, there is another parametrization in the paper by Vácha et al. [64] in which the behavior of H_2O_2 at the air-water interface was investigated. The force field by Vácha et al. [64] only includes electrostatic and van der Waals interactions which were calibrated against the experimental hydration energies of H_2O_2. H_2O_2 exhibits internal cis-trans rotation with an energy barrier of about 4.6 kJ/mol [71,72]. This is about 2 k_BT (k_B is the Boltzmann constant and T is the temperature) at room temperature. A realistic model of hydrogen peroxide should incorporate the energy barrier for the internal cis-trans rotation of the molecule. This is the case for the force field by Orabi & English [67] and the force field by Cordeiro [69]. The force field by Vácha et al. [64] does not allow this rotation to occur.

In this manuscript, we evaluate the quality of the force fields which were developed by Cordeiro [69], and Orabi & English [67] for predicting the thermodynamic properties of H_2O_2 in aqueous solutions. We exclude the force field by Vácha et al. [64] from our study as it is unable to capture the internal rotation that takes place in H_2O_2 at ambient conditions. We compute the densities of pure H_2O_2 for a range of temperatures (253 K to 353 K), and compare the results with experimental values. In addition, we compute densities, viscosities, and self-diffusion coefficients of H_2O_2 and water in aqueous solutions of H_2O_2 for the whole range of H_2O_2 mole fractions at ambient temperatures and pressures.

To evaluate which water force field is suitable for predicting properties of aqueous solutions of H_2O_2, we use four different widely used water force fields: TIP3P [73,68], TIP5P-E [74], TIP4P/2005 [75], and a modified version of TIP3P (mTIP3P) [68] that was used in the original work by Orabi & English [67]. The TIP3P [73,68] force field is able to predict the densities and heats of vaporization of water at ambient conditions, it performs better in calculating the specific heats of water [74], and it also predicts the excess chemical potential of water in better agreement with the experimental values compared to TIP4P/2005 and TIP5P-E [76]. TIP5P-E can capture the thermal conductivities of water [74] and its maximum density near 4 °C [77]. TIP4P/2005 [75,78] can predict the densities and self-diffusion coefficients of water with commendable accuracy [75]. The results are compared with experimental values. Finally, we compute the Henry coefficients of H_2O_2 in water at 300 K and 1 bar.

The rest of this manuscript is organized as follows. In section 2, details of the force fields which were developed by Cordeiro [69], and Orabi & English [67] are provided, and the MD and CFCMC simulations are described. The results are presented and discussed in section 3. Finally, concluding remarks are presented in section 4.

2. Methodology

2.1. Force fields

The force fields developed by Cordeiro [69] and Orabi & English [67] for H_2O_2 both use potential energy functions for bonded interactions (i.e., bonds, angles, and dihedrals) as well as non-bonded interactions, including van der Waals (vdW) and electrostatic interactions. The total potential energy (E_{total}) is given by

$$E_{total} = E_{bonds} + E_{angles} + E_{dihedrals} + E_{vdW} + E_{electrostatic}, \quad (1)$$

Table 1
Potential energy functions for force fields developed by Cordeiro [69], and Orabi & English [67]. E_{bonds}, E_{angles}, $E_{\text{dihedrals}}$, E_{vdW}, and $E_{\text{electrostatic}}$ represent the stretching, bending, torsional, van der Waals and electrostatic energies, respectively. The definition of parameters is explained in the text (see section 2.1). The parameters are provided in Tables S1 and S2 of the Supplementary Information.

Force field	Cordeiro [69]	Orabi & English [67]
E_{bonds}	$\frac{1}{4}k_b(b^2-b_0{}^2)^2$	$\frac{1}{2}k_b(b-b_0)^2$
E_{angle}	$\frac{1}{2}k_\theta(\cos\theta-\cos\theta_0)^2$	$\frac{1}{2}k_\theta(\theta-\theta_0)^2$
$E_{\text{dihedrals}}$	$\sum_{n=0}^{5} C_n(\cos\psi)^n$	$k_\phi(1+\cos 2\phi-\delta)$
E_{vdW}	$4\epsilon_{ij}[(\frac{\sigma_{ij}}{r_{ij}})^{12}-(\frac{\sigma_{ij}}{r_{ij}})^{6}]$	$4\epsilon_{ij}[(\frac{\sigma_{ij}}{r_{ij}})^{12}-(\frac{\sigma_{ij}}{r_{ij}})^{6}]$
$E_{\text{electrostatic}}$	$\frac{1}{4\pi\epsilon_o}\frac{q_iq_j}{r_{ij}}$	$\frac{1}{4\pi\epsilon_o}\frac{q_iq_j}{r_{ij}}$

where E_{bonds}, E_{angles}, $E_{\text{dihedrals}}$, E_{vdW}, and $E_{\text{electrostatic}}$ are presented in Table 1 for both force fields. The bonded interaction parameters (E_{bonds}, E_{angles}, and $E_{\text{dihedrals}}$) listed in Table 1 have the following definitions: b is the bond distance, θ is the bond angle, ϕ is the dihedral angle, δ is the multiplicity factor, and ψ is the supplementary angle of ϕ. k_b, k_θ, k_ϕ are the force constants of the bond stretching, angle vibration, and dihedral potentials. b_0 and θ_0 represent the bond distance and bond angle, respectively, at which the corresponding potential functions equal zero. C_n with n ranging from 0 to 5 represents the coefficients for the Ryckaert-Bellemans dihedral potential [79]. q represents the atomic partial charges of the electrostatic energy ($E_{\text{electrostatic}}$) term. A Lennard-Jones (L-J) potential is used for the long-range van der Waals interactions, in which σ represents the distance at which the particle-particle interaction energy is zero, and ϵ represents the depth of the potential well. The mixing rules for the L-J parameters for two dissimilar non-bonded atoms are given by Lorentz-Berthelot [80] [$\sigma_{ij}=\frac{\sigma_i+\sigma_j}{2}$, $\epsilon_{ij}=\sqrt{\epsilon_i\epsilon_j}$] for the force field by Orabi & English and geometric average [$\sigma_{ij}=\sqrt{\sigma_i\sigma_j}$, $\epsilon_{ij}=\sqrt{\epsilon_i\epsilon_j}$] for the force field by Cordeiro. The values of these parameters are provided (using the GROMACS convention) in Tables S1 and S2 of the Supporting Information (SI) for both force fields. The cutoff radius for Lennard-Jones and Coulombic interactions was set to 9 Å. The Particle-Mesh-Ewald [81,82] method was used to treat long-range electrostatic interactions. Long-range tail corrections were applied to both energies and pressures [83].

We use three different rigid water force fields in this study, namely TIP3P, [73,68] TIP4P/2005, [75] and TIP5P-E [77,84]. We also use a modified TIP3P water force field (mTIP3P) [68] which was used in the work by Orabi & English [67]. In the remainder of this manuscript, the force field developed by Cordeiro [69] is referred to as "Cordeiro" and the force field developed by Orabi & English [67] is referred to as "Orabi".

2.2. MD simulations

All-atom Molecular Dynamics (MD) simulation of anhydrous H_2O_2 for a range of temperatures from 253 K to 353 K, and H_2O_2 aqueous solutions for various mole fractions of H_2O_2 in the range from 0 to 1.0 at 298 K, were performed using the GROningen MAchine for Chemical Simulations (GROMACS) version 2022.4 [85–89]. Each system was prepared in a simulation box with an initial length of 27.6 Å, containing 500 molecules. A snapshot of a simulation box containing 250 H_2O_2 molecules and 250 H_2O molecules is shown in Fig. 1.

After energy minimization using the steepest descent algorithm followed by a conjugate gradient algorithm, the MD simulations were run for 100 ps in the constant number of atoms/molecules, volume and temperature (NVT) ensemble. The simulations were then continued in the constant number of atoms/molecules, pressure and temperature (NPT) ensemble for 25 ns. For calculating the viscosities and self-diffusivities, the simulations were continued in the NVT ensemble for another 20 ns. The temperature was kept fixed by Nosé-Hoover thermostat [90]. The

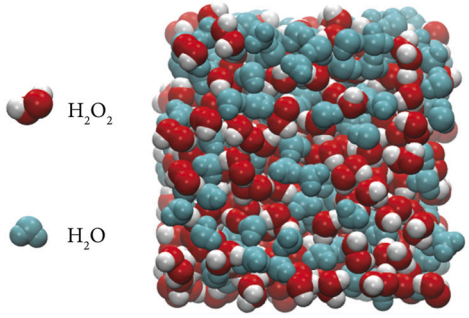

Fig. 1. A snapshot of a simulation box containing 250 H_2O_2 (red and white spheres represent oxygen and hydrogen atoms, respectively) and 250 H_2O molecules (green spheres), generated by the Visual Molecular Dynamic (VMD) software [95].

Parinello-Rahman barostat [91] with a time constant of 1 ps and compressibility of 4.5×10^{-5} bar^{-1} was used to keep the pressure at 1 bar. In all simulations, the Newton's equations of motion were integrated with a leap-frog [92] algorithm with a time step of 2 fs. Periodic boundary conditions were applied in all Cartesian directions. The parallel linear constraint solver (P-LINCS) [93,94] was used to constrain the O–H bonds in the H_2O_2 molecule. In this way, the fastest degree of freedom in H_2O_2 (O–H vibrations), is removed which allows to safely use 2 fs time step in our MD simulations.

2.3. MC simulations

Continuous Fractional Component Monte Carlo (CFCMC) simulations [96–98] using the open-source Brick-CFCMC software [98–100] were performed in the isothermal-isobaric (NPT) ensemble. In the CFCMC technique, fractional molecules (compared to normal or "whole" molecules) are introduced whose interactions with the rest of the system are scaled with a continuous coupling parameter λ ($\lambda\in[0,1]$). The minimum value of λ ($\lambda=0$) indicates no interactions between the fractional molecule and the rest of the molecules in the system (i.e., fractional molecules act as ideal gas molecules). $\lambda=1$ represents full interactions between the fractional molecules and the other molecules in the system (i.e., the fractional molecule acts as whole molecules). The coupling parameter λ is biased with a weight function ($W(\lambda)$) using the Wang-Landau algorithm [101] to improve molecule transfers (insertions/deletions). This ensures a smooth observed probability distribution of λ. We used 100 bins to construct a histogram for the λ values and its probability of occurrence (p(λ)). The Boltzmann average of any property (A) is then computed using [102]

$$\langle A\rangle=\frac{\langle A\exp[-W(\lambda)]\rangle_{\text{biased}}}{\langle\exp[-W(\lambda)]\rangle_{\text{biased}}}. \tag{2}$$

The chemical potential of species i is calculated with respect to its ideal gas chemical potential [99]

$$\mu_i=\mu_i^{\text{ideal}}+\mu_i^{\text{ex}}, \tag{3}$$

where μ_i^{ideal} and μ_i^{ex} are the ideal gas and excess chemical potential of the species i, respectively. The excess chemical potential can be related to the Boltzmann sampled probability distribution of λ by the following equation [99]

$$\mu_i^{\text{ex}}=-k_{\text{B}}T\ln\frac{p(\lambda=1)}{p(\lambda=0)}, \tag{4}$$

where $p(\lambda=1)$ and $p(\lambda=0)$ are the Boltzmann sampled probability distributions of λ at 1 and 0, respectively. k_{B} is the Boltzmann constant, and T is the absolute temperature. The excess chemical potential at in-

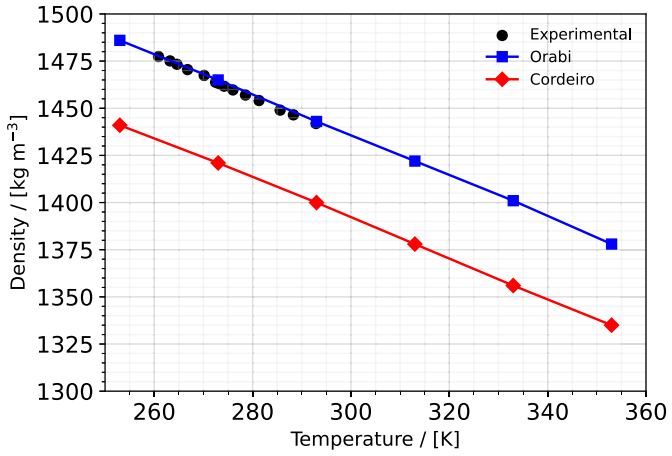

Fig. 2. Densities of anhydrous H_2O_2 at various temperatures using the Cordeiro [69] and Orabi [67] force fields at 1 bar with the experimental values [42]. Error bars are estimated based on the standard deviation and are much smaller than the symbols used in the figure.

finite dilution ($\mu^{ex,\infty}$) can be used to determine the Henry volatility coefficient[1] (K_v^{px}) by [104]

$$K_v^{px} = \rho\, k_B T \exp\left(\frac{\mu^{ex,\infty}}{k_B T}\right), \tag{5}$$

where ρ is the number density of the solvent. This yields the Henry volatility coefficient (K_v^{px}) in units of [Pa]. The Henry coefficient (H_s^{cp}) in units of [mol/m^3 Pa] can be obtained using the following conversion: $H_s^{cp} \approx \frac{\rho_{H_2O}}{M_{H_2O} K_v^{px}}$ in which ρ_{H_2O} is the density of water, and M_{H_2O} is the molar mass of water [103]. The Henry coefficient (H_s^{cp}) will have the SI units only if ρ, k_B, T, and M are in SI units.

CFCMC simulations contained 300 water molecules in a cubic simulation box with initial dimensions of 21 Å. A single fractional molecule of H_2O_2 was introduced to calculate its excess chemical potential. The cut-off radius for the intermolecular L-J and Coulombic interactions was set to 9 Å. The Ewald summation [105] method was used for calculating electrostatic interactions. Long-range tail corrections were applied to the L-J potential. Periodic boundary conditions were applied in all directions.

For CFCMC simulations, 1,000 initialization cycles were carried out followed by 5×10^6 equilibration cycles and 5×10^6 production cycles. One cycle refers to N number of trial moves, where N is the total number of molecules. Trial moves were selected with the following probabilities: 32% translation moves, 22% rotation moves, 1% volume changes, 5% each of bending and torsion moves, 25% λ changes, and 10% hybrid moves that combined swap and identity change moves [99]. Three independent simulations were performed for each combination of water force field and H_2O_2 force field to obtain an average value and the standard deviation for the Henry coefficients.

3. Results and discussion

3.1. Densities

The densities of anhydrous H_2O_2 for a temperature range of 253 K to 353 K (in steps of 20 K) for both the Orabi and Cordeiro force fields are plotted in Fig. 2. We used the *gmx density* tool to compute the average density of each system. The experimental values are shown in black circles [42]. The melting point and boiling point of H_2O_2 are reported as 272.74 K and 423.15 K, respectively [106]. While the Cordeiro force field underestimates the densities of anhydrous H_2O_2 by about 3% compared to the experimental values, the densities of anhydrous H_2O_2 using the Orabi force field are in excellent agreement with the experimental values.

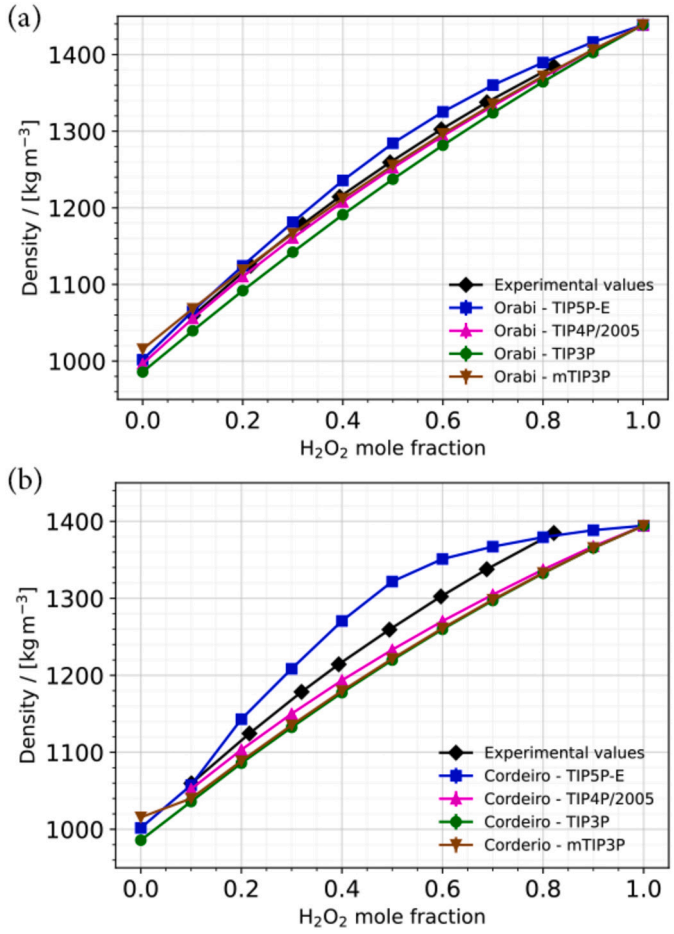

Fig. 3. Densities of H_2O_2 aqueous solution for various mole fractions of H_2O_2 at $T = 298$ K and 1 bar using the (a) Orabi [67] and (b) Cordeiro [69] force fields in combination with the TIP3P [73], mTIP3P [68], TIP4P/2005 [75] and TIP5P-E [77,84] water force fields. Experimental values [50] are added for comparison. Error bars are estimated based on the standard deviation and are much smaller than the symbols used in the figure.

Next, we evaluate which water force field is suitable for predicting the densities of H_2O_2 aqueous solutions. To this end, we modelled systems of H_2O_2 aqueous solutions for the whole range of H_2O_2 mole fractions (0 to 1.0) at $T = 298$ K and 1 bar using the Orabi or Cordeiro force fields in combination with four different water force fields: TIP3P, TIP4P/2005, TIP5P-E, and the modified TIP3P water force field (mTIP3P) which was used in the work by Orabi & English [67]. The choice of temperature at 298 K and pressure at 1 bar was motivated by the availability of experimental results by which we could validate our models. The results as a function of the H_2O_2 mole fraction are shown in Fig. 3. The experimental values [50] are added for comparison.

The densities of pure water (i.e., a mole fraction of zero), using the four water force fields are in good agreement with the reported data at 298 K and 1 bar [75,107]. The Orabi force field for H_2O_2 in combination with the TIP4P/2005 water force field or mTIP3P water force field predicts the densities of the aqueous solutions in good agreement (ca. 0.6%) with the experimental values [50]. The predicted values for densities of solutions using the TIP5P-E water force field in combination with the Orabi or Cordeiro force fields at low and high concentrations

[1] The definition of the Henry law constants is according to Sander [103].

of H_2O_2 are in good agreement with the experimental values. At intermediate concentrations (0.4 - 0.6 mole fractions), however, the TIP5P-E in combination with the Orabi or Cordeiro force fields overestimates the densities of solutions by 2% and 5%, respectively. The TIP3P water force field in combination with the Orabi force field underestimates the densities of the solutions by 2%. The Cordeiro-TIP3P and Cordeiro-mTIP3P models underestimate the densities by 3% at intermediate concentrations. The Cordeiro force field in combination with the TIP4P/2005 water force field also underestimates the densities of the solution with a more pronounced effect at higher mole fractions of H_2O_2 (≥ 0.5, by 3%).

We conclude that the Orabi force field is a better force field than the Cordeiro force field for predicting the densities of pure H_2O_2 in the temperature range of 253 - 353 K. In addition, the TIP4P/2005 or the mTIP3P force field in combination with the Orabi force field predicts the densities of H_2O_2 aqueous solutions for the whole range of mole fractions (0 - 1.0) in very good agreement with the experimental values.

3.2. Viscosities

The viscosities were calculated by a non-equilibrium molecular dynamics (NEMD) method, available within GROMACS. For a Newtonian liquid, an applied external force induces a velocity gradient in the system, according to the Navier-Stokes equation. From the constitutive relation between the response strain rate and applied shear stress, we can determine the viscosity of the liquid [108]. In our study, we used an amplitude of 0.02 nm/ps^2 for the acceleration profile. The viscosities of H_2O_2 aqueous solutions for various H_2O_2 mole fractions (0 to 1.0) at $T = 293$ K were computed. Fig. 4 shows the values of viscosity using the Orabi (a) and Cordeiro (b) force fields in combination with the TIP3P, mTIP3P and TIP4P/2005 force fields. The results including the TIP5P-E water force field are shown in Figure S1 of the Supplementary Information. The standard deviation is used to estimate error bars. The experimental values at 293 K are included for comparison [43].

The viscosities of pure water (i.e., mole fraction = 0) are in good agreement with the computed values using the TIP3P, mTIP3P, TIP4P/2005, and TIP5P-E force fields [109]. The experimental value of the viscosity of pure H_2O_2 at 293 K is 1.25 mPa s [43]. The computed value is 1.36 mPa s by using the Orabi force field, and it is 1.34 mPa s by using the Cordeiro force field.

The combination of the Orabi force field with the mTIP3P or TIP4P/2005 underestimates the viscosities of H_2O_2 aqueous solutions for mole fractions up to 0.9. The Orabi-TIP3P model underestimates the values up to a mole fraction of 0.8, above which it slightly overestimates. The combination of Cordeiro force field with the mTIP3P or TIP3P or TIP4P/2005 water force fields follows a similar trend. The Cordeiro-mTIP3P and Cordeiro-TIP3P models underestimate the viscosities up to a mole fraction of 0.8, above which it slightly overestimates. The Cordeiro-TIP4P/2005 model, however, underestimates the values of viscosities by 7% up to a mole fraction of 0.5 while it overestimates by ca. 5% for H_2O_2 mole fractions higher than 0.8. Contrary to the other water force fields, the TIP5P-E water force field in combination with either the Orabi or Cordeiro force fields predicts a relatively high peak in viscosity at the intermediate mole fractions (mole fraction of 0.5), see Figure S1 of the Supplementary Information. This may be due to structural changes which the TIP5P-E water force field induces in the system. This is addressed in section 3.4 using radial distribution functions.

We conclude that the TIP4P/2005 water force field in combination with the Orabi force field or the Cordeiro force field predicts the viscosities of H_2O_2 aqueous solutions in better agreement with the experimental values.

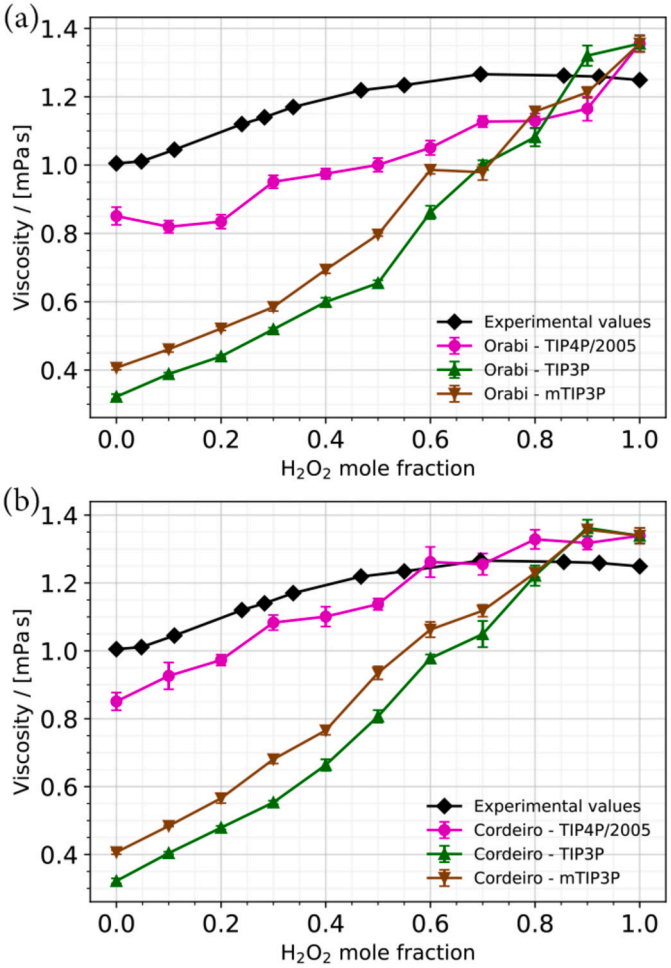

Fig. 4. Viscosities of H_2O_2 aqueous solution for various mole fractions of H_2O_2 at 293 K for the (a) Orabi [67] and (b) Cordeiro [69] force fields in combination with the TIP3P [73], mTIP3P [68] and TIP4P/2005 [75]. The results including the TIP5P-E water force field are shown in Figure S1 of the Supplementary Information. Error bars are estimated based on the standard deviation. The experimental values [43] at 293 K are added for comparison.

3.3. Self-diffusion coefficients

Diffusion coefficients were calculated from the mean-squared displacements (MSD) and were corrected for finite-size effects with the Yeh-Hummer equation [110,111]

$$D = D_{\mathrm{MD}} + \frac{k_{\mathrm{B}} T \xi}{6\pi\eta L}, \tag{6}$$

where D and D_{MD} denote the diffusion coefficient calculated with and without the finite-size effects corrections, respectively. k_{B} is the Boltzmann constant, T is the absolute temperature (in K), ξ is a dimensionless number which for a cubic simulation box is equal to 2.837, L is the length of the cubic simulation box, and η is the viscosity of the system. We used the *gmx msd* tool to obtain the MSD as a function of time. D_{MD} is obtained by fitting the MSD to

$$\langle r^2 \rangle_{\mathrm{MSD}} = 2d\, D_{\mathrm{MD}} t, \tag{7}$$

where $d = 3$ is the dimension of the system. The self-diffusion coefficients were calculated from 1 ns to 20 ns NVT trajectories. Figure S3 of the SI shows an example of MSD versus time on a logarithmic scale. Fig. 5 shows the self-diffusion coefficients of H_2O_2 and water in aqueous H_2O_2 solutions for the whole range of hydrogen peroxide mole fractions (0 to 1.0). The results including the TIP5P-E water force

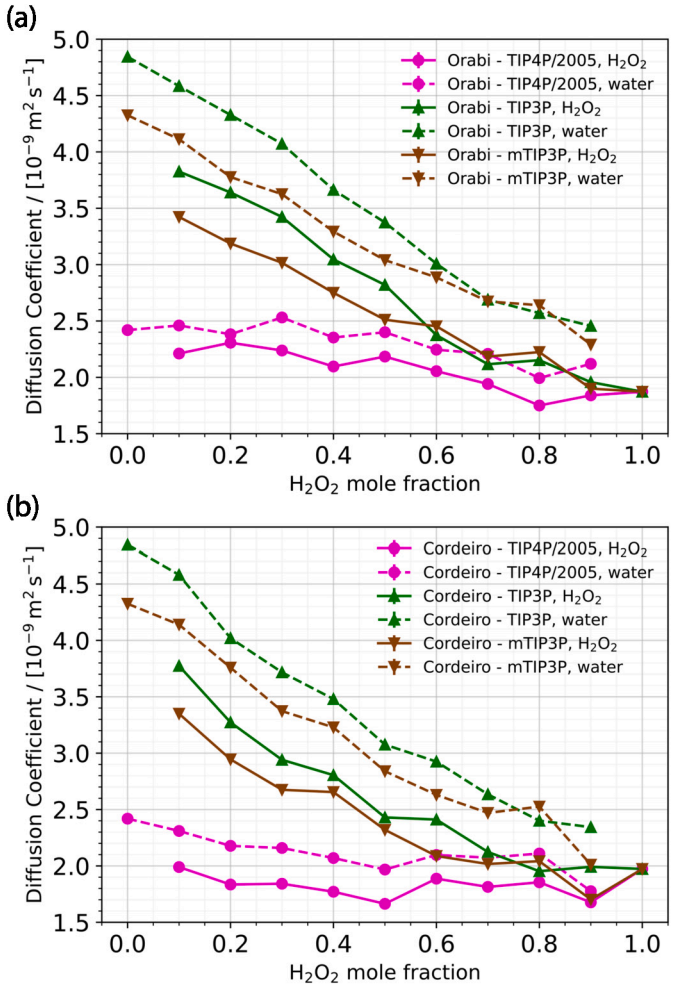

Fig. 5. Self-diffusion coefficients of water molecules and H_2O_2 molecules in H_2O_2 aqueous solutions for different mole fractions of H_2O_2 at 298 K using the (a) Orabi [67] and (b) Cordeiro [69] force fields in combination with the TIP3P [73], mTIP3P [68], and TIP4P/2005 [75] water force fields. The results including the TIP5P-E water force field are shown in Figure S2 of the Supplementary Information. Error bars are estimated based on the standard deviation and are much smaller than the symbols used in the figure.

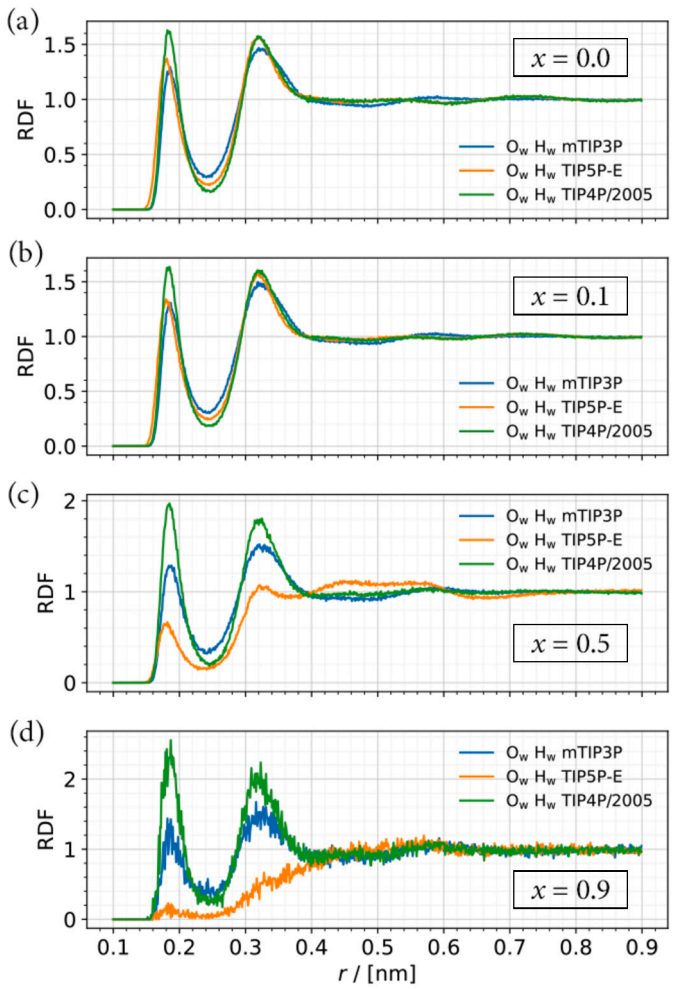

Fig. 6. Radial distribution functions (RDFs) as a function of radial distance, r [nm], for O_w (O of water) - H_w (H of water) for H_2O_2 aqueous solutions with $x = 0.1$ (b), $x = 0.5$ (c), and $x = 0.9$ (d) at 298 K and 1 bar using the Orabi force field in combination with the mTIP3P [68], TIP5P-E [77,84], and TIP4P/2005 [75] water force fields, where x is the mole fraction of H_2O_2. The RDF for pure water is plotted in (a).

field are shown in Figure S2 of the SI. The self-diffusion coefficients of pure water (i.e., mole fraction = 0) for the four water force fields are in good agreement with the values reported in Ref. [75,112,77]. The TIP5P-E and TIP4P/2005 water force fields predict the value of the self-diffusion coefficient in better agreement with the experimental value (2.3 nm^2/s [113]).

The self-diffusion coefficients of both the water and the H_2O_2 molecules decrease monotonically by increasing the mole fraction of H_2O_2 using the Orabi-TIP3P or Orabi-mTIP3P models. There is a similar trend for the Cordeiro-TIP3P and Cordeiro-mTIP3P models. The TIP4P/2005 water force field in combination with either the Orabi force field or the Cordeiro force field predicts a relatively constant self-diffusion coefficient for both water and H_2O_2 for the whole range of mole fractions. This is in agreement with a recent experimental study [33] where it was concluded that the self-diffusion coefficients of H_2O_2 in solutions are insensitive to its concentration. The TIP5P-E water force field in combination with either the Orabi or Cordeiro force fields predicts a minimum at a mole fraction of 0.5 for the self-diffusion coefficients of both water and H_2O_2. This is correlated with its very high value of viscosities (see Figure S1 of the Supplementary Information).

3.4. Radial distribution functions

In sections 3.2 and 3.3, we concluded that the TIP5P-E water force field in combination with either the Orabi force field or the Cordeiro force field for H_2O_2 does not predict viscosities of H_2O_2 aqueous solutions, and thereby self-diffusion coefficients of H_2O_2 in aqueous solution, well. To identify the reason behind, structural properties of H_2O_2 aqueous solution at various mole fractions were investigated using the radial distribution functions (RDF), and hydrogen bonding pattern were explored. Note that there are 4 atom types in each system: hydrogen of water (H_w), oxygen of water (O_w), hydrogen of H_2O_2 (H_p), and oxygen of H_2O_2 (O_p).

The RDFs for O_w and H_w in pure water using the mTIP3P, TIP5P-E and TIP4P/2005 water force fields are shown in Fig. 6 (a). The results show a first peak at approximately 0.18 nm, and a second peak at approximately 0.32 nm. The peak heights slightly differ between the water force fields with the TIP4P/2005 predicting a higher value followed by the TIP5P-E, and then the mTIP3P predicting a smaller value.

The respective RDFs in H_2O_2 aqueous solutions using the Orabi force field in combination with the three water force fields for systems with mole fractions of 0.1, 0.5, and 0.9 are also shown in Fig. 6 (b, c, d). The RDFs for O_w and H_w for systems using the Cordeiro force field in combination with the mTIP3P, TIP5P-E, and TIP4P/2005 are shown in Figure

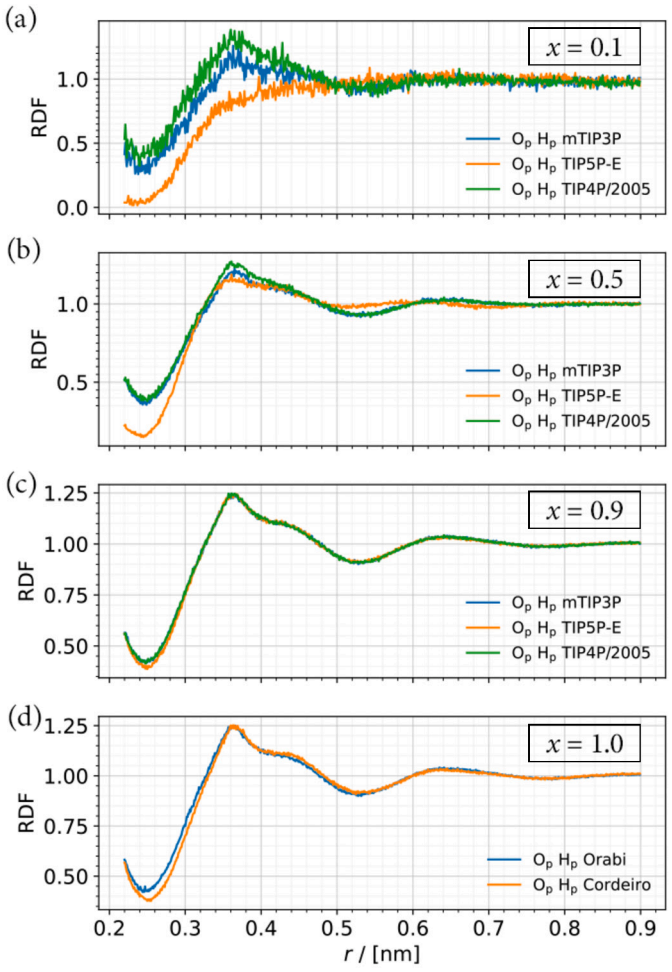

Fig. 7. Radial distribution functions (RDFs) as a function of radial distance, r [nm], for O_p (O of H_2O_2) - H_p (H of H_2O_2) for H_2O_2 aqueous solutions with $x = 0.1$ (b), $x = 0.5$ (c), and $x = 0.9$ (d) at 298 K and 1 bar using the Orabi [67] force field in combination with the mTIP3P [68], TIP5P-E [77,84], and TIP4P/2005 [75] water force fields, where x is the mole fraction of H_2O_2. The first peak (at ca. 0.19 nm) was removed to distinguish the differences between the combinations clearly. The RDF for pure H_2O_2 is plotted in (d) using the Orabi force field and the Cordeiro force field.

S4 of the SI. In the system with a mole fraction of 0.1, the position of the peaks is independent of the water force fields. As the mole fraction of H_2O_2 is increased to 0.5 and 0.9, the position of the peaks does not change in systems where the mTIP3P or TIP4P/2005 force field is used. In the systems where the TIP5P-E water force field is used, however, the RDF changes: the height of the peaks becomes smaller and an additional structural correlation appears in the system with a mole fraction of 0.5. This additional correlation between the water molecules persists till 0.8 nm, whereas for the systems in which the mTIP3P or TIP4P/2005 is used, the structural correlation persists only till 0.6 nm. In the Orabi-TIP5P-E system with a mole fraction 0.9, the first two peaks disappear. A similar trend can be observed for the combinations involving the Cordeiro force field with the mTIP3P, TIP5P-E, and TIP4P/2005 water force fields (see Figure S4 of SI). In the Cordeiro-TIP5P-E combination with a mole-fraction of 0.5, however, the structural correlation between the water molecules is stronger than that of the corresponding Orabi-TIP5P-E combination. This can be seen from a more prominent peak after 0.4 nm compared to the other models.

The RDFs for O_p and H_p in H_2O_2 aqueous solution with mole fractions of 0.1, 0.5 and 0.9 using the Orabi force field in combination with the three water force fields are shown in Fig. 7 (a, b, c). Similarly, the respective RDFs using the Cordeiro force field in combination with the three water force fields are shown in Figure S5 of SI. The RDF of O_p and H_p in pure H_2O_2 using the Orabi and the Cordeiro force fields are also shown in Fig. 7 (d). The first peak in the RDF has a large amplitude, therefore we removed it to be able to distinguish the differences between the systems more clearly (see Figure S6 of SI). RDFs of the system at a mole fraction of 0.9 are almost identical using the three different water force fields with a second peak at 0.37 nm. By decreasing the mole fraction of H_2O_2 to 0.5, and 0.1, the RDFs remain the same for the systems in which the mTIP3P-E or the TIP4P/2005 is used. For the system in which the TIP5P-E water force field is used, however, the RDF changes drastically. This is also the case with the Cordeiro-TIP5P-E model. The RDF for pure H_2O_2 using the Orabi force field is almost identical as the system using the Cordeiro force field.

The RDFs for O_p and H_w, O_p and O_w, and O_w and H_p using the Orabi force field with the three water force fields (mTIP3P, TIP4P/2005, and TIP5P-E) for solutions with mole fractions of 0.1, 0.5 and 0.9, are shown in Fig. 8. Likewise, RDFs with the Cordeiro force field and the water force fields are shown in Figure S7 of SI. In systems where the mTIP3P and TIP4P/2005 water force fields were used, RDFs have the same structure in which the position of the first peak is in good agreement with X-ray measurements on crystals of $H_2O_2{\cdot}2H_2O$ [114] and simulation results [67]. On the contrary, the structural properties in systems where the TIP5P-E force field was used, have changed. A comparable effect can be seen in Figure S7 of SI where the Cordeiro-TIP5P-E combination is used.

The number of water molecules in the micro and first solvation shells of H_2O_2 molecule were obtained by integrating up to the first and second minima of the RDF for O_p - O_w, respectively. The results are shown in Table S3 and S4 of the SI. Orabi & English [67] reported 3.0 and 9.4 water molecules in the micro and first solvation shells, respectively, for a single peroxide molecule in 500 water molecules using the mTIP3P water force field. Authors in Ref. [58] report 6.0 water molecules in the first solvation shell of H_2O_2 using a hybrid quantum-classical simulation. According to our results, the number of water molecules in the first solvation shell at mole fractions of 0.1 and 0.9 are lower for systems where the TIP5P-E water force field is used. At a mole fraction of 0.5, however, the number of water molecules in the first solvation shell slightly increases.

3.5. Hydrogen bond analysis

The number of hydrogen bonds (calculated as the summation of hydrogen bonds between H_2O_2 - H_2O_2, H_2O_2 - water and water - water) per H_2O_2 molecule for combinations of the Orabi and Cordeiro force fields with the water force fields is shown in Fig. 9. We used the geometric criterion for hydrogen bonds proposed in Ref. [115]. Accordingly, a hydrogen bond is identified when the angle formed by the hydrogen, the acceptor, and donor atoms is below 30°, with the distance between the acceptor and donor atoms to be less than 0.36 nm. The geometric criterion is depicted in Figure S8 of the SI. The number of hydrogen bonds for both the Orabi and Cordeiro force fields in combination with the TIP4P/2005, TIP3P and mTIP3P water force fields exhibit a steady increase until a mole fraction of 0.9. Existing literature indicates the existence of about 4 hydrogen bonds between hydrogen peroxide and water molecules [58,60]. For pure H_2O_2 systems, the number of hydrogen bonds sharply decreases to about 5 for both the Orabi and Cordeiro systems. The Orabi-TIP5P-E and Cordeiro-TIP5P-E combinations are however different compared to the others. These combinations indicate a minimum in the number of hydrogen bonds at a mole fraction of 0.4 (around 3 hydrogen bonds for Orabi-TIP5P-E and 2 for Cordeiro-TIP5P-E). The minima for the number of hydrogen bonds at the intermediate concentrations for both these systems are concurrent with the high viscosities and low diffusion seen in Figures S1 and S2 of the SI.

Analysis of the RDFs, solvation shells, and the number of hydrogen bonds of the TIP5P-E systems indicate a variation in the arrangement

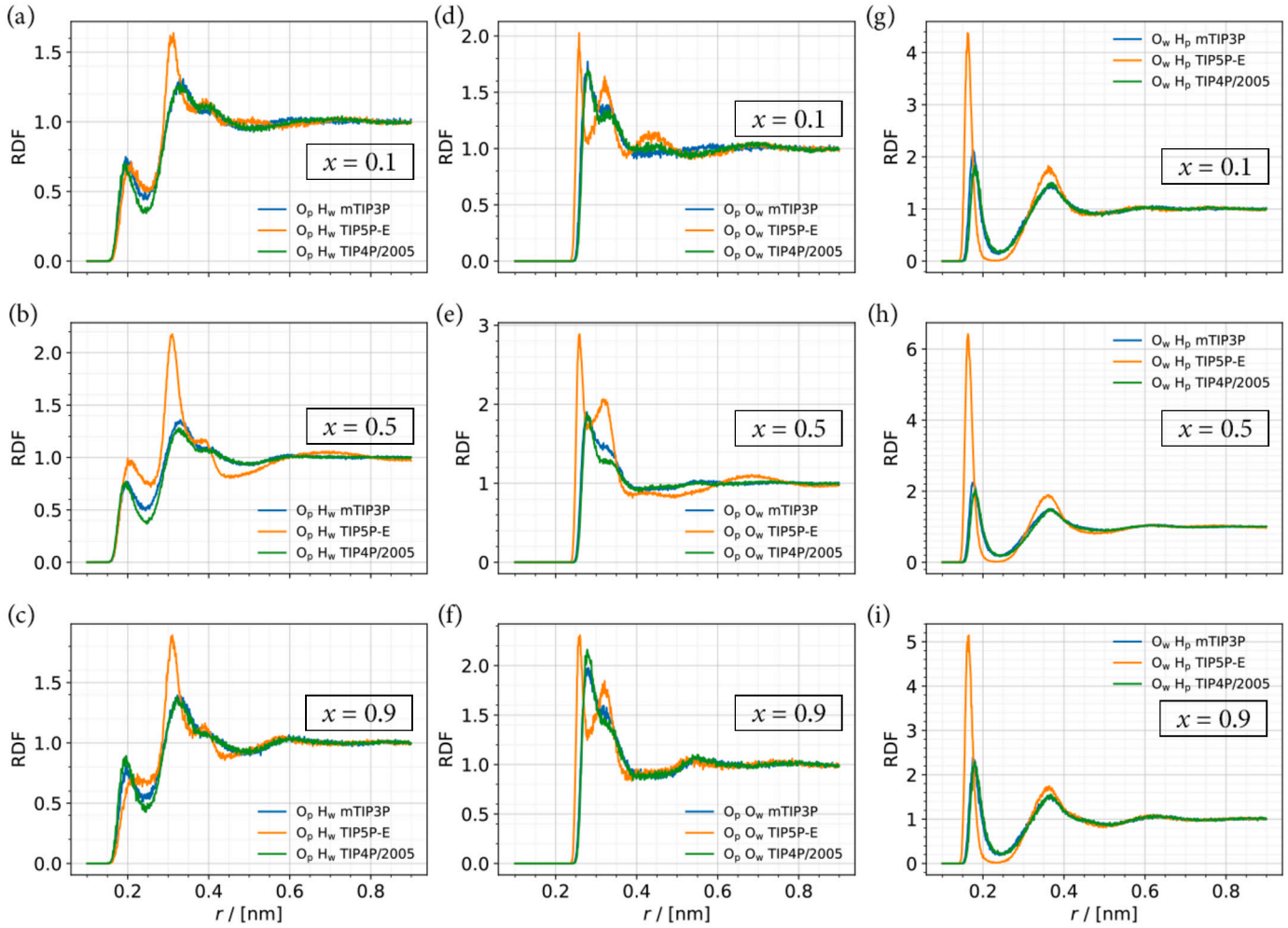

Fig. 8. Radial distribution functions (RDFs) as a function of radial distance, r [nm], for O_p (O of H_2O_2) and H_w (H of water) (a - c), O_w (O of water) and O_p (O of H_2O_2) (d - f), and O_w (O of water) and H_p (H of H_2O_2) (g - i) for systems using the mTIP3P [68], TIP5P-E [77,84], and TIP4P/2005 [75] water force fields in combination with the Orabi force field for $x = 0.1$, $x = 0.5$, and $x = 0.9$ at 298 K and 1 bar, where x is the mole fraction of H_2O_2.

of water molecules around a H_2O_2 molecule. We attribute this to the presence of the two dummy atoms representing the lone electron pairs of the oxygen atom of the water molecule in the TIP5P-E water force field. This is in agreement with the work by Nutt and Smith [116] who compared the performance of three water force fields, TIP5P, TIP4P, and mTIP3P in providing a reliable description for protein solvation in water. These authors concluded that TIP5P behaves differently from TIP4P and mTIP3P as the RDFs between the hydrogen of the protein and oxygen of water for their protein-TIP5P system exhibit a shift in the peak position and peak heights, similar to the RDFs in our systems (see Fig. 8 (g-i)). This anomalous behavior of TIP5P was attributed to the presence of the two dummy atoms representing the lone electron pairs of the oxygen atom of the water molecule in TIP5P. As we observed the same trend in our aqueous systems of H_2O_2, we conclude that the combination of the TIP5P-E water force field and either of the H_2O_2 force fields induce stronger interactions between the water molecules and H_2O_2 due to the presence of the two dummy atoms representing the lone electron pairs of the oxygen atom of the water molecule using the TIP5P-E water force field. This leads to the incongruity of the viscosities and self-diffusion coefficients of the TIP5P-E systems compared to the other systems.

3.6. Henry coefficients

The Henry coefficients were computed for H_2O_2 in water using the Orabi and Cordeiro force fields in combination with the various water force fields. It should be noted that we have not further considered the TIP5P-E water force field for the solubility calculations as it has been ascertained from the earlier sections that neither the Cordeiro nor Orabi force fields in combination with the TIP5P-E water force field could accurately predict the densities, viscosities and self-diffusion coefficients of H_2O_2 aqueous systems. The results of the solubility calculations are provided in Table 2. The reported experimental values range from 670 to 1400 [mol/m^3 Pa] [117–120]. It is evident that the Cordeiro force field in combination with the TIP3P or mTIP3P water force fields predicts the Henry constants that are within the range of the reported experimental values.

Table 2
Excess chemical potentials (μ^{ex}), the Henry volatility coefficient (K_v^{px}), and the Henry coefficient (H_s^{cp}), using the Orabi and the Cordeiro force fields in combination with the TIP4P/2005, TIP3P, and mTIP3P water force fields. Errors are estimated using standard deviations of independent simulations.

Model	μ^{ex}/[K]	K_v^{px}/[Pa]	H_s^{cp}/[mol/m^3 Pa]
Orabi - TIP4P/2005	−3734 ± 30	512 ± 52	109 ± 11
Orabi - TIP3P	−3836 ± 27	365 ± 32	153 ± 14
Orabi - mTIP3P	−3963 ± 14	239 ± 11	232 ± 11
Cordeiro - TIP4P/2005	−4142 ± 32	132 ± 14	424 ± 46
Cordeiro - TIP3P	−4392 ± 58	58 ± 11	989 ± 190
Cordeiro - mTIP3P	−4487 ± 57	42 ± 7	1357 ± 275

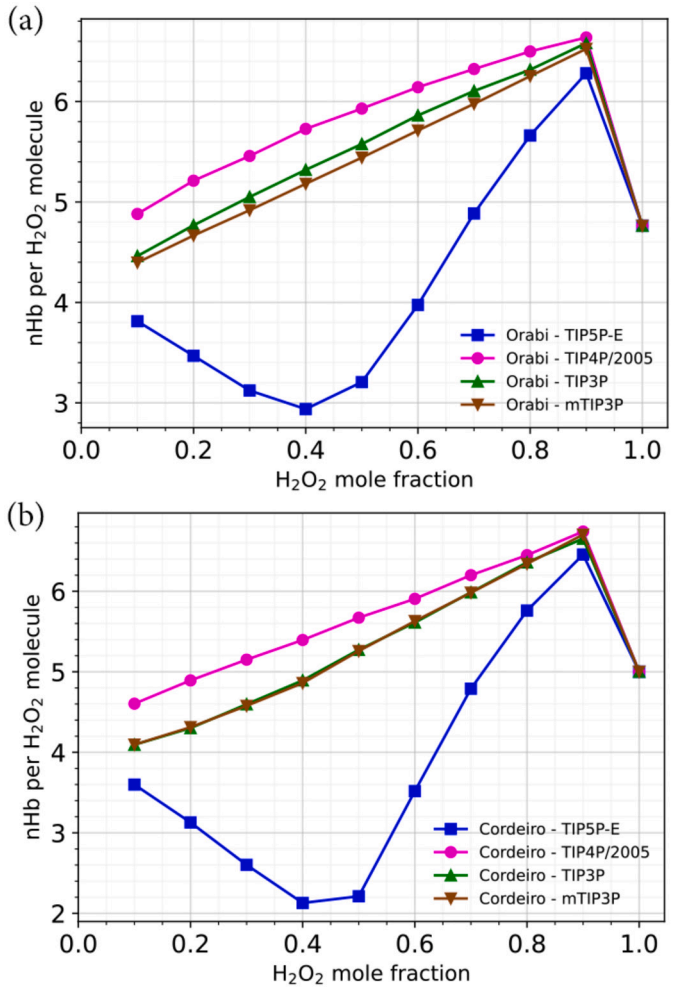

Fig. 9. Number of hydrogen bonds per H_2O_2 molecule for systems with various mole fractions of H_2O_2 at $T = 298$ K and 1 bar using the (a) Orabi [67] and (b) Cordeiro [69] force fields in combination with the TIP3P [73], mTIP3P [68], TIP4P/2005 [75] and TIP5P-E [77,84] water force fields.

4. Conclusions

We performed MD and CFCMC simulations to study thermodynamic properties of aqueous solutions of H_2O_2. The quality of the available force fields of H_2O_2, Cordeiro [69] and Orabi [67], was evaluated by comparing the results with experiments. The densities of pure H_2O_2 computed using the Orabi force field are in excellent agreement with the experimental values for the temperature range of 253 K to 353 K. The Cordeiro force field underestimates the densities of pure H_2O_2 by 3%. We computed densities, viscosities, and self-diffusion coefficients of H_2O_2 in aqueous solutions for the whole range of mole fractions of H_2O_2 (0 to 1.0) at ambient temperatures and pressures using four widely used water force fields: TIP3P, mTIP3P, TIP4P/2005, and TIP5P-E. The results show that the TIP4P/2005 water force field in combination with the Orabi force field can predict the densities of H_2O_2 aqueous solution in excellent agreement with experimental values. Both the Orabi and Cordeiro force fields in combination with the TIP4P/2005 water force field predict the viscosities of H_2O_2 in reasonable agreement with experimental results. The TIP5P-E water force field leads to a very high value (maximum) for viscosity of H_2O_2 aqueous solutions at a mole fraction of 0.5, and thereby a very small value (minimum) for self-diffusion coefficient of H_2O_2 and water. The TIP4P/2005 force field in combination with either of the Orabi or Cordeiro force fields predicts a relatively constant diffusion coefficient for the whole range of H_2O_2 mole fractions that is in agreement with a recent experimental study [33]. Analysis of the RDFs, solvation shells, and the number of hydrogen bonds of the TIP5P-E systems indicate a variation in the arrangement of water molecules around a H_2O_2 molecule. We attribute this to the presence of the two dummy atoms representing the lone electron pairs of the oxygen atom of the water molecule in the TIP5P-E water force field, which leads to a stronger interaction between water molecules and H_2O_2 molecules and therefore a deviation in the dynamic properties (viscosities and self-diffusion coefficients) of these systems. Finally, we computed the Henry coefficients of H_2O_2 in water. The values using the Cordeiro force field in combination with either of the TIP3P or mTIP3P water force fields are within the range of experimental values. The quantitative data presented in this work can be used by macroscopic plasma fluid models to determine the uptake of H_2O_2 from the gas phase plasma by liquid [36] or to interpret and complement experimental findings [121].

CRediT authorship contribution statement

Tijin H.G. Saji: Conceptualization, Formal analysis, Investigation, Writing – original draft. **José Manuel Vicent-Luna:** Formal analysis, Writing – review & editing. **Thijs J.H. Vlugt:** Formal analysis, Methodology, Writing – review & editing, Software. **Sofía Calero:** Methodology, Writing – review & editing, Formal analysis. **Behnaz Bagheri:** Conceptualization, Formal analysis, Funding acquisition, Investigation, Methodology, Project administration, Supervision, Writing – original draft, Writing – review & editing.

Declaration of competing interest

The authors declare that they have no known competing financial interests or personal relationships that could have appeared to influence the work reported in this paper.

Data availability

The input files to run MD and CFCMC simulations are provided at https://zenodo.org/doi/10.5281/zenodo.10600369.

Acknowledgements

BB thanks the strategic alliance between TU/e, Utrecht University, and University Medical Center Utrecht, and TS thanks the Institute for Complex Molecular Systems for financial support.

Appendix A. Supplementary material

Supplementary material related to this article can be found online at https://doi.org/10.1016/j.molliq.2024.124530.

References

[1] J. Lelieveld, P. Crutzen, Influences of cloud photochemical processes on tropospheric ozone, Nature 343 (1990) 227–233.
[2] P.J. Crutzen, M.G. Lawrence, U. Pöschl, On the background photochemistry of tropospheric ozone, Tellus, Ser. B Chem. Phys. Meteorol. 51 (1999) 123–146.
[3] R.J. Lewis, G.J. Hutchings, Recent advances in the direct synthesis of H_2O_2, ChemCatChem 11 (2019) 298–308.
[4] Z. Chen, D. Yao, C. Chu, S. Mao, Photocatalytic H_2O_2 production systems: design strategies and environmental applications, Chem. Eng. J. 451 (2023) 138489.
[5] J. Wang, Y. Zhang, E. Archibong, F.S. Ligler, Z. Gu, Leveraging H_2O_2 levels for biomedical applications, Adv. Biosyst. 1 (2017) 1700084.
[6] D. Möller, Atmospheric hydrogen peroxide: evidence for aqueous-phase formation from a historic perspective and a one-year measurement campaign, Atmos. Environ. 43 (2009) 5923–5936.
[7] D. Vione, V. Maurino, C. Minero, E. Pelizzetti, et al., The atmospheric chemistry of hydrogen peroxide: a review, Ann. Chim. 93 (2003) 477.
[8] M. Lee, B.G. Heikes, D.W. O'Sullivan, Hydrogen peroxide and organic hydroperoxide in the troposphere: a review, Atmos. Environ. 34 (2000) 3475–3494.
[9] M. Hoffmann, J. Edwards, Kinetics of the oxidation of sulfite by hydrogen peroxide in acidic solution, J. Phys. Chem. 79 (1975) 2096–2098.

[10] S. Penkett, B. Jones, K. Brich, A.E. Eggleton, The importance of atmospheric ozone and hydrogen peroxide in oxidising sulphur dioxide in cloud and rainwater, Atmos. Environ. (1967) 13 (1979) 123–137.

[11] L.R. Martin, D.E. Damschen, Aqueous oxidation of sulfur dioxide by hydrogen peroxide at low pH, Atmos. Environ. (1967) 15 (1981) 1615–1621.

[12] D.E. Damschen, L.R. Martin, Aqueous aerosol oxidation of nitrous acid by O_2, O_3 and H_2O_2, Atmos. Environ. (1967) 17 (1983) 2005–2011.

[13] J.G. Calvert, A. Lazrus, G.L. Kok, B.G. Heikes, J.G. Walega, J. Lind, C.A. Cantrell, Chemical mechanisms of acid generation in the troposphere, Nature 317 (1985) 27–35.

[14] L.I. Kleinman, Seasonal dependence of boundary layer peroxide concentration: the low and high NO_x regimes, J. Geophys. Res., Atmos. 96 (1991) 20721–20733.

[15] J.A. Logan, M.J. Prather, S.C. Wofsy, M.B. McElroy, Tropospheric chemistry: a global perspective, J. Geophys. Res., Oceans 86 (1981) 7210–7254.

[16] H. Levy, Normal atmosphere: large radical and formaldehyde concentrations predicted, Science 173 (1971) 141–143.

[17] J. Fierro, J.M. Campos-Martin, G. Blanco-Brieva, Hydrogen peroxide synthesis: an outlook beyond the anthraquinone process angewandte, Angew. Chem., Int. Ed. 45 (2006) 6962–6984.

[18] J.M. Campos-Martin, G. Blanco-Brieva, J.L. Fierro, Hydrogen peroxide synthesis: an outlook beyond the anthraquinone process, Angew. Chem., Int. Ed. 45 (2006) 6962–6984.

[19] H. Hou, X. Zeng, X. Zhang, Production of hydrogen peroxide by photocatalytic processes, Angew. Chem., Int. Ed. 59 (2020) 17356–17376.

[20] K. Mase, M. Yoneda, Y. Yamada, S. Fukuzumi, Seawater usable for production and consumption of hydrogen peroxide as a solar fuel, Nat. Commun. 7 (2016) 11470.

[21] Y. Kofuji, Y. Isobe, Y. Shiraishi, H. Sakamoto, S. Tanaka, S. Ichikawa, T. Hirai, Carbon nitride–aromatic diimide–graphene nanohybrids: metal-free photocatalysts for solar-to-hydrogen peroxide energy conversion with 0.2% efficiency, J. Am. Chem. Soc. 138 (2016) 10019–10025.

[22] S. Fukuzumi, Production of liquid solar fuels and their use in fuel cells, Joule 1 (2017) 689–738.

[23] E.S. Shanley, F.P. Greenspan, Highly concentrated hydrogen peroxide, Ind. Eng. Chem. 39 (1947) 1536–1543.

[24] S.C. Perry, S. Mavrikis, L. Wang, C.P. de León, Future perspectives for the advancement of electrochemical hydrogen peroxide production, Curr. Opin. Electrochem. 30 (2021) 100792.

[25] C. Samanta, Direct synthesis of hydrogen peroxide from hydrogen and oxygen: an overview of recent developments in the process, Appl. Catal. A, Gen. 350 (2008) 133–149.

[26] R. Burch, P. Ellis, An investigation of alternative catalytic approaches for the direct synthesis of hydrogen peroxide from hydrogen and oxygen, Appl. Catal. B, Environ. 42 (2003) 203–211.

[27] G. Genti, R. Dittmeyer, S. Perathoner, M. Reif, Tubular inorganic catalytic membrane reactors: advantages and performance in multiphase hydrogenation reactions, Catal. Today 79 (2003) 139.

[28] P. Bruggeman, C. Leys, Non-thermal plasmas in and in contact with liquids, J. Phys. D, Appl. Phys. 42 (2009) 053001.

[29] P.J. Bruggeman, F. Iza, R. Brandenburg, Foundations of atmospheric pressure non-equilibrium plasmas, Plasma Sources Sci. Technol. 26 (2017) 123002.

[30] A.A. Joshi, B.R. Locke, P. Arce, W.C. Finney, Formation of hydroxyl radicals, hydrogen peroxide and aqueous electrons by pulsed streamer corona discharge in aqueous solution, J. Hazard. Mater. 41 (1995) 3–30.

[31] B.R. Locke, K.-Y. Shih, Review of the methods to form hydrogen peroxide in electrical discharge plasma with liquid water, Plasma Sources Sci. Technol. 20 (2011) 034006.

[32] Y.F. Yue, S. Mohades, M. Laroussi, X. Lu, Measurements of plasma-generated hydroxyl and hydrogen peroxide concentrations for plasma medicine applications, IEEE Trans. Plasma Sci. 44 (2016) 2754–2758.

[33] M. Suresh, V.S.K. Kondeti, P.J. Bruggeman, Production and diffusion of H_2O_2 during the interaction of a direct current pulsed atmospheric pressure plasma jet on a hydrogel, J. Phys. D, Appl. Phys. 55 (2022) 185201.

[34] F. Cameli, P. Dimitrakellis, T.-Y. Chen, D.G. Vlachos, Modular plasma microreactor for intensified hydrogen peroxide production, ACS Sustain. Chem. Eng. 10 (2022) 1829–1838.

[35] P. Bruggeman, M.J. Kushner, B.R. Locke, J.G. Gardeniers, W. Graham, D.B. Graves, R. Hofman-Caris, D. Maric, J.P. Reid, E. Ceriani, et al., Plasma–liquid interactions: a review and roadmap, Plasma Sources Sci. Technol. 25 (2016) 053002.

[36] W. Tian, M.J. Kushner, Atmospheric pressure dielectric barrier discharges interacting with liquid covered tissue, J. Phys. D, Appl. Phys. 47 (2014) 165201.

[37] P.A. Giguère, V. Schomaker, An electron diffraction study of hydrogen peroxide and hydrazine, J. Am. Chem. Soc. 65 (1943) 2025–2029.

[38] P. Giguere, T. Srinivasan, A Raman study of H_2O_2 and D_2O_2 vapor, J. Raman Spectrosc. 2 (1974) 125–132.

[39] S. Abrahams, R. Collin, W. Lipscomb, The crystal structure of hydrogen peroxide, Acta Crystallogr. 4 (1951) 15–20.

[40] J.M. Savariault, M. Lehmann, Experimental determination of the deformation electron density in hydrogen peroxide by combination of X-ray and neutron diffraction measurements, J. Am. Chem. Soc. 102 (1980) 1298–1303.

[41] C. Fritchie, R. McMullan, Neutron diffraction study of the 1: 1 urea: hydrogen peroxide complex at 81 K, Acta Crystallogr., Sect. B, Struct. Crystallogr. Cryst. Chem. 37 (1981) 1086–1091.

[42] O. Maass, W.H. Hatcher, The properties of pure hydrogen peroxide. I, J. Am. Chem. Soc. 42 (1920) 2548–2569.

[43] M. Phibbs, P.A. Giguère, Hydrogen peroxide and its analogues: I. Density, refractive index, viscosity, and surface tension of deuterium peroxide–deuterium oxide solutions, Can. J. Chem. 29 (1951) 173–181.

[44] R. Redington, W. Olson, P. Cross, Studies of hydrogen peroxide: the infrared spectrum and the internal rotation problem, J. Chem. Phys. 36 (1962) 1311–1326.

[45] J. Koput, On the r_0^* structure and the torsional potential function of hydrogen peroxide, J. Mol. Spectrosc. 115 (1986) 438–441.

[46] G. Khachkuruzov, I. Przhevalskii, Molecular constants of hydrogen peroxide. 7: Parameters of the potential energy of internal rotation, Opt. Spectrosc. 44 (1978) 112–114.

[47] R.H. Hunt, R.A. Leacock, C.W. Peters, K.T. Hecht, Internal-rotation in hydrogen peroxide: the far-infrared spectrum and the determination of the hindering potential, J. Chem. Phys. 42 (1965) 1931–1946.

[48] O. Maass, P. Hiebert, The properties of pure hydrogen peroxide. v. Vapor pressure, J. Am. Chem. Soc. 46 (1924) 2693–2700.

[49] W.T. Foley, P.A. Giguère, Hydrogen peroxide and its analogues: IV. Some thermal properties of hydrogen peroxide, Can. J. Chem. 29 (1951) 895–903.

[50] M.F. Easton, A.G. Mitchell, W.F.K. Wynne-Jones, The behaviour of mixtures of hydrogen peroxide and water. Part 1.—Determination of the densities of mixtures of hydrogen peroxide and water, Trans. Faraday Soc. 48 (1952) 796–801.

[51] W.T. Foley, P.A. Giguère, Hydrogen peroxide and its analogues: II. Phase equilibrium in the system hydrogen peroxide–water, Can. J. Chem. 29 (1951) 123–132.

[52] G. Scatchard, G.M. Kavanagh, L.B. Ticknor, Vapor-liquid equilibrium. VIII. Hydrogen peroxide—water mixtures, J. Am. Chem. Soc. 74 (1952) 3715–3720.

[53] D. Cremer, Theoretical determination of molecular structure and conformation. I. The role of basis set and correlation effects in calculations on hydrogen peroxide, J. Chem. Phys. 69 (1978) 4440–4455.

[54] J. Koput, S. Carter, N.C. Handy, Potential energy surface and vibrational- rotational energy levels of hydrogen peroxide, J. Phys. Chem. A 102 (1998) 6325–6330.

[55] S.A. Kulkarni, L.J. Bartolotti, R.K. Pathak, Ab initio investigations on neutral hydrogen peroxide clusters: (H_2O_2) n (n= 2–4), Chem. Phys. Lett. 372 (2003) 620–626.

[56] M. Elango, R. Parthasarathi, V. Subramanian, C. Ramachandran, N. Sathyamurthy, Hydrogen peroxide clusters: the role of open book motif in cage and helical structures, J. Phys. Chem. A 110 (2006) 6294–6300.

[57] A.D. Kulkarni, R.K. Pathak, L.J. Bartolotti, Structures, energetics, and vibrational spectra of $H_2O_2 \cdots (H_2O)$ n, n= 1- 6 clusters: ab initio quantum chemical investigations, J. Phys. Chem. A 109 (2005) 4583–4590.

[58] S.T. Moin, T.S. Hofer, B.R. Randolf, B.M. Rode, An ab initio quantum mechanical charge field molecular dynamics simulation of hydrogen peroxide in water, Comput. Theor. Chem. 980 (2012) 15–22.

[59] C. Ferreira, H.F. Martiniano, B.J.C. Cabral, V. Aquilanti, Electronic excitation and ionization of hydrogen peroxide–water clusters: comparison with water clusters, Int. J. Quant. Chem. 111 (2011) 1824–1835.

[60] A. Priyadarsini, B.S. Mallik, Structure and rotational dynamics of water around hydrogen peroxide, J. Mol. Liq. 348 (2022) 118054.

[61] L. Domínguez, A. Sosa-Peinado, W. Hansberg, Catalase evolved to concentrate H_2O_2 at its active site, Arch. Biochem. Biophys. 500 (2010) 82–91.

[62] Y.-H. Chung, J. Xia, C.J. Margulis, Diffusion and residence time of hydrogen peroxide and water in crowded protein environments, J. Phys. Chem. B 111 (2007) 13336–13344.

[63] L. Domínguez, A. Sosa-Peinado, W. Hansberg, How catalase recognizes H_2O_2 in a sea of water, Proteins 82 (2014) 45–56.

[64] R. Vácha, P. Slavíček, M. Mucha, B.J. Finlayson-Pitts, P. Jungwirth, Adsorption of atmospherically relevant gases at the air/water interface: free energy profiles of aqueous solvation of N_2, O_2, O_3, OH, H_2O, HO_2, and H_2O_2, J. Phys. Chem. A 108 (2004) 11573–11579.

[65] Z.-Z. Yang, C.-S. Wang, Atom-bond electronegativity equalization method. 1. Calculation of the charge distribution in large molecules, J. Phys. Chem. A 101 (1997) 6315–6321.

[66] C.-S. Wang, Z.-Z. Yang, Atom–bond electronegativity equalization method. II. Lone-pair electron model, J. Chem. Phys. 110 (1999) 6189–6197.

[67] E.A. Orabi, A.M. English, A simple additive potential model for simulating hydrogen peroxide in chemical and biological systems, J. Chem. Theory Comput. 14 (2018) 2808–2821.

[68] E. Neria, S. Fischer, M. Karplus, Simulation of activation free energies in molecular systems, J. Chem. Phys. 105 (1996) 1902–1921.

[69] R.M. Cordeiro, Reactive oxygen species at phospholipid bilayers: distribution, mobility and permeation, Biochim. Biophys. Acta, Biomembr. 1838 (2014) 438–444.

[70] M. de Swart, M. Van den Bosch, H. Berendsen, G. Canters, J. Snijders, Density functional theory and molecular dynamics results for copper proteins, J. Inorg. Biochem. 86 (2001) 445.

[71] J.-M. Flaud, C. Camy-Peyret, J. Johns, B. Carli, The far infrared spectrum of h2o2. First observation of the staggering of the levels and determination of the cis barrier, J. Chem. Phys. 91 (1989) 1504–1510.

[72] A. Biswas, B.S. Mallik, Conformational dynamics of aqueous hydrogen peroxide from first principles molecular dynamics simulations, Phys. Chem. Chem. Phys. 22 (2020) 28286–28296.
[73] W.L. Jorgensen, J. Chandrasekhar, J.D. Madura, R.W. Impey, M.L. Klein, Comparison of simple potential functions for simulating liquid water, J. Chem. Phys. 79 (1983) 926–935.
[74] Y. Mao, Y. Zhang, Thermal conductivity, shear viscosity and specific heat of rigid water models, Chem. Phys. Lett. 542 (2012) 37–41.
[75] J.L. Abascal, C. Vega, A general purpose model for the condensed phases of water: TIP4P/2005, J. Chem. Phys. 123 (2005) 234505.
[76] A. Rahbari, J. Brenkman, R. Hens, M. Ramdin, L.J. Van Den Broeke, R. Schoon, R. Henkes, O.A. Moultos, T.J. Vlugt, Solubility of water in hydrogen at high pressures: a molecular simulation study, J. Chem. Eng. Data 64 (2019) 4103–4115.
[77] S.W. Rick, A reoptimization of the five-site water potential (TIP5P) for use with Ewald sums, J. Chem. Phys. 120 (2004) 6085–6093.
[78] P. Florová, P. Sklenovsky, P. Banas, M. Otyepka, Explicit water models affect the specific solvation and dynamics of unfolded peptides while the conformational behavior and flexibility of folded peptides remain intact, J. Chem. Theory Comput. 6 (2010) 3569–3579.
[79] J.-P. Ryckaert, A. Bellemans, Molecular dynamics of liquid alkanes, Faraday Discuss. Chem. Soc. 66 (1978) 95–106.
[80] H.A. Lorentz, Ueber die Anwendung des Satzes vom Virial in der kinetischen Theorie der Gase, Ann. Phys. 248 (1881) 127–136.
[81] T. Darden, D. York, L. Pedersen, Particle mesh Ewald: an n· log (n) method for Ewald sums in large systems, J. Chem. Phys. 98 (1993) 10089–10092.
[82] U. Essmann, L. Perera, M.L. Berkowitz, T. Darden, H. Lee, L.G. Pedersen, A smooth particle mesh Ewald method, J. Chem. Phys. 103 (1995) 8577–8593.
[83] D. Frenkel, B. Smit, Understanding Molecular Simulation: from Algorithms to Applications, 3rd ed., Elsevier, 2023.
[84] M.W. Mahoney, W.L. Jorgensen, A five-site model for liquid water and the reproduction of the density anomaly by rigid, nonpolarizable potential functions, J. Chem. Phys. 112 (2000) 8910–8922.
[85] M.J. Abraham, T. Murtola, R. Schulz, S. Páll, J.C. Smith, B. Hess, E. Lindahl, Gromacs: high performance molecular simulations through multi-level parallelism from laptops to supercomputers, SoftwareX 1 (2015) 19–25.
[86] E. Lindahl, B. Hess, D. Van Der Spoel, Gromacs 3.0: a package for molecular simulation and trajectory analysis, Mol. Model. Annu. 7 (2001) 306–317.
[87] D. Van Der Spoel, E. Lindahl, B. Hess, G. Groenhof, A.E. Mark, H.J. Berendsen, Gromacs: fast, flexible, and free, J. Comput. Chem. 26 (2005) 1701–1718.
[88] B. Hess, C. Kutzner, D. Van Der Spoel, E. Lindahl, Gromacs 4: algorithms for highly efficient, load-balanced, and scalable molecular simulation, J. Chem. Theory Comput. 4 (2008) 435–447.
[89] S. Pronk, S. Páll, R. Schulz, P. Larsson, P. Bjelkmar, R. Apostolov, M.R. Shirts, J.C. Smith, P.M. Kasson, D. van der Spoel, B. Hess, E. Lindahl, GROMACS 4.5: a high-throughput and highly parallel open source molecular simulation toolkit, Bioinformatics (Oxford, England) 29 (2013) 845–854.
[90] W.G. Hoover, Canonical dynamics: equilibrium phase-space distributions, Phys. Rev. A 31 (1985) 1695–1697.
[91] M. Parrinello, A. Rahman, Polymorphic transitions in single crystals: a new molecular dynamics method, J. Appl. Phys. 52 (1981) 7182–7190.
[92] R.W. Hockney, J.W. Eastwood, Computer Simulation Using Particles, CRC Press, Boca Raton, 2021.
[93] B. Hess, H. Bekker, H.J. Berendsen, J.G. Fraaije, Lincs: a linear constraint solver for molecular simulations, J. Comput. Chem. 18 (1997) 1463–1472.
[94] B. Hess, P-lincs: a parallel linear constraint solver for molecular simulation, J. Chem. Theory Comput. 4 (2008) 116–122.
[95] W. Humphrey, A. Dalke, K. Schulten, VMD: visual molecular dynamics, J. Mol. Graph. 14 (1996) 33–38.
[96] W. Shi, E.J. Maginn, Continuous fractional component Monte Carlo: an adaptive biasing method for open system atomistic simulations, J. Chem. Theory Comput. 3 (2007) 1451–1463.
[97] W. Shi, E.J. Maginn, Improvement in molecule exchange efficiency in Gibbs ensemble Monte Carlo: development and implementation of the continuous fractional component move, J. Comput. Chem. 29 (2008) 2520–2530.
[98] A. Rahbari, R. Hens, M. Ramdin, O.A. Moultos, D. Dubbeldam, T.J.H. Vlugt, Recent advances in the continuous fractional component Monte Carlo methodology, Mol. Simul. 47 (2021) 804–823.
[99] R. Hens, A. Rahbari, S. Caro-Ortiz, N. Dawass, M. Erdős, A. Poursaeidesfahani, H.S. Salehi, A.T. Celebi, M. Ramdin, O.A. Moultos, D. Dubbeldam, T.J.H. Vlugt, Brick-CFCMC: open source software for Monte Carlo simulations of phase and reaction equilibria using the continuous fractional component method, J. Chem. Inf. Model. 60 (2020) 2678–2682.
[100] H.M. Polat, H.S. Salehi, R. Hens, D.O. Wasik, A. Rahbari, F. de Meyer, C. Houriez, C. Coquelet, S. Calero, D. Dubbeldam, O.A. Moultos, T.J.H. Vlugt, New features of the open source Monte Carlo software Brick-CFCMC: thermodynamic integration and hybrid trial moves, J. Chem. Inf. Model. 61 (2021) 3752–3757.
[101] F. Wang, D.P. Landau, Efficient, multiple-range random walk algorithm to calculate the density of states, Phys. Rev. Lett. 86 (2001) 2050–2053.
[102] A. Poursaeidesfahani, A. Torres-Knoop, D. Dubbeldam, T.J.H. Vlugt, Direct free energy calculation in the continuous fractional component Gibbs ensemble, J. Chem. Theory Comput. 12 (2016) 1481–1490.
[103] R. Sander, Compilation of Henry's law constants (version 4.0) for water as solvent, Atmos. Chem. Phys. 15 (2015) 4399–4981.
[104] H.S. Salehi, R. Hens, O.A. Moultos, T.J.H. Vlugt, Computation of gas solubilities in choline chloride urea and choline chloride ethylene glycol deep eutectic solvents using Monte Carlo simulations, J. Mol. Liq. 316 (2020) 113729.
[105] B.A. Wells, A.L. Chaffee, Ewald summation for molecular simulations, J. Chem. Theory Comput. 11 (2015) 3684–3695.
[106] P.A. Giguère, Molecular association and structure of hydrogen peroxide, J. Chem. Educ. 60 (1983) 399.
[107] C. Vega, J. Abascal, Relation between the melting temperature and the temperature of maximum density for the most common models of water, J. Chem. Phys. 123 (2005) 144504.
[108] B. Hess, Determining the shear viscosity of model liquids from molecular dynamics simulations, J. Chem. Phys. 116 (2002) 209–217.
[109] M.A. González, J.L. Abascal, The shear viscosity of rigid water models, J. Chem. Phys. 132 (2010) 096101.
[110] I.-C. Yeh, G. Hummer, System-size dependence of diffusion coefficients and viscosities from molecular dynamics simulations with periodic boundary conditions, J. Phys. Chem. B 108 (2004) 15873–15879.
[111] A.T. Celebi, S.H. Jamali, A. Bardow, T.J.H. Vlugt, O.A. Moultos, Finite-size effects of diffusion coefficients computed from molecular dynamics: a review of what we have learned so far, Mol. Simul. 47 (2021) 831–845.
[112] P. Mark, L. Nilsson, Structure and dynamics of the TIP3P, SPC, and SPC/E water models at 298 K, J. Phys. Chem. A 105 (2001) 9954–9960.
[113] M. Holz, S.R. Heil, A. Sacco, Temperature-dependent self-diffusion coefficients of water and six selected molecular liquids for calibration in accurate ^{1}H NMR PFG measurements, Phys. Chem. Chem. Phys. 2 (2000) 4740–4742.
[114] I. Olovsson, D.H. Templeton, The crystal structure of hydrogen peroxide dihydrate, Acta Chem. Scand. 14 (1960) 1325–1332.
[115] A. Luzar, D. Chandler, Structure and hydrogen bond dynamics of water–dimethyl sulfoxide mixtures by computer simulations, J. Chem. Phys. 98 (1993) 8160–8173.
[116] D.R. Nutt, J.C. Smith, Molecular dynamics simulations of proteins: can the explicit water model be varied?, J. Chem. Theory Comput. 3 (2007) 1550–1560.
[117] H. Hwang, P.K. Dasgupta, Thermodynamics of the hydrogen peroxide-water system, Environ. Sci. Technol. 19 (1985) 255–258.
[118] K. Yoshizumi, K. Aoki, I. Nouchi, T. Okita, T. Kobayashi, S.K. Amakura, M. Tajima, Measurements of the concentration in rainwater and of the Henry's law constant of hydrogen peroxide, Atmos. Environ. (1967) 18 (1984) 395–401.
[119] X. Zhou, Y.N. Lee, Aqueous solubility and reaction kinetics of hydroxymethyl hydroperoxide, J. Phys. Chem. 96 (1992) 265–272.
[120] D. Huang, Z. Chen, Reinvestigation of the Henry's law constant for hydrogen peroxide with temperature and acidity variation, J. Environ. Sci. 22 (2010) 570–574.
[121] Z. Machala, B. Tarabová, D. Sersenová, M. Janda, K. Hensel, Chemical and antibacterial effects of plasma activated water: correlation with gaseous and aqueous reactive oxygen and nitrogen species, plasma sources and air flow conditions, J. Phys. D, Appl. Phys. 52 (2018) 034002.